Effects of the Cr-depletion on the stress state of the sublayer of ni-base alloys oxidized in high temperature water

Benoît Ter-Ovanessian, Eric Andrieu, Dominique Poquillon, Alexandre Freulon, Jean-Marc Cloué

DOI 10.1007/s11085-012-9327-1

Effects of the Cr-Depletion on the Stress State of the Sublayer of Ni-Base Alloys Oxidized in High Temperature Water

B. Ter-Ovanessian · E. Andrieu · D. Poquillon · A. Freulon · J.-M. Cloué

Abstract The exposure in high-temperature water (300–360 °C) of Alloy 600 is known to induce not only generalized corrosion, but also degradation at the underlying base metal such as intergranular penetrations of oxygen and\or oxides and Cr-depletion. Possible consequences of Cr-depletion are the creation of local stresses in the underlying metal due to local variations of the lattice parameter, and the formation of physicals properties gradient, like the elastic modulus or thermal expansion coefficient. In order to assess the effects caused by the Cr-depletion on an exposed Alloy 600, finite element (FE) calculations and physical properties characterisations on synthetic alloys with a chemical composition representative of different Cr-depleted layers, were performed. The levels of the calculated stresses were then discussed regarding to the other features of oxidation involved in the high temperature water stress-corrosion cracking mechanism.

Keywords High temperature water · Cr-depletion · Nickel alloy · SCC

Introduction

The nickel-based alloys, widely used due to their good corrosion resistance, are known to be sensitive to environmentally-induced intergranular stress corrosion cracking (IGSCC) in high temperature water [1–4]. Some of the numerous models proposed to describe the damaging process, assumed that the oxidation process is at

J.-M. Cloué: At Present, Senior Expert at AREVA Group.

B. Ter-Ovanessian (✉)
MATEIS-CorrIS, INSA de Lyon, 21 Avenue Jean Capelle, 69621 Villeurbanne Cedex, France
e-mail: benoit.ter-ovanessian@insa-lyon.fr

E. Andrieu · D. Poquillon · A. Freulon · J.-M. Cloué
CIRIMAT, CNRS/UPS/INPT, ENSIACET, 4, allée Emile Monso, 31030 Toulouse, France

the origin of the IGSCC initiation [4–10]. Therefore, the characterization of the oxidation features as well as their roles appears of major importance for understanding the nickel-based alloys susceptibility. As commonly admitted results, the consequences of the exposure in high temperature water may be summarized by three main findings: the formation and the growth of a multi-layer oxide scale [6, 8–11], the intergranular penetration of oxygen deep under the interface metal/oxide [6, 7, 9, 10, 12, 13], and the selective oxidation of Cr inducing Cr-depleted zones in the underlying metal and at the oxygen penetration tips [6, 8–13]. Since the other phenomena have been extensively studied, the occurrence of Cr-depleted zones has to be considered in the IGSCC degradation mechanisms.

Firstly, Cr-depletion has been reported to be detrimental to protective film repair kinetics. Indeed, as the formation of the passive film is dependent on the Cr content, such Cr-depleted zones are unfavourable to the repassivation required in case of accidental film break down. Secondly, Cr-depletion is assumed to generate local stresses due to volume changes. Cr content variations have effectively a direct impact on the lattice parameter [14]. Thus, the Cr gradient between the base metal and the different layers of the Cr-depleted zone induce volume changes which may generate a significant stress state [6, 15]. These local stresses could be cumulated with the surface stresses created by the oxide layer growth, and might be involved in the initiation of SCC cracks [6, 15]. Moreover, Cr content variation has also an effect on the coefficient of thermal expansion and their differences contribute to the former local stress state, in particular in the case of a cooling down.

The aim of the present study is to evaluate the consequences of Cr-depletion occurring into the underlying metal of Alloy 600 exposed to simulated primary water of pressurized water reactor (PWR) by finite elements (FE) calculations coupled with experimental characterisations.

For the purpose of characterising the Cr-depletion, the chemical composition variations in the Cr-depleted zone were determined from a previous study [9]. A commercial Alloy 600, was exposed during 300 h to simulated primary water (deionized and deaerated water + 1200 ppm B (weight) as boric acid (H_3BO_3) + 2 ppm Li (weight) as lithium hydroxide (LiOH), + 0.3 bar H_2 partial pressure) at 360 °C. After exposure, energy-dispersive X-ray spectrometry (EDX) was performed in a transmission electron microscope (TEM) on a polished cross-section (Fig. 1) of the oxidized alloy.

Experimental Procedures

For this study, three alloys were used: the previous Alloy 600 and two synthetic NiCrFe alloys with a chemical composition chosen to be representative of two layers of the Cr-depleted zone (Fig. 1). The nominal composition of the alloys studied is given in Table 1.

Coupons of Alloy 600 were extracted from a mill-annealed square plate (980 °C/4 min + cooling under hydrogen atmosphere) and then heat treated in an inert atmosphere for 2 h at 820 °C. The microstructure was characterized by a

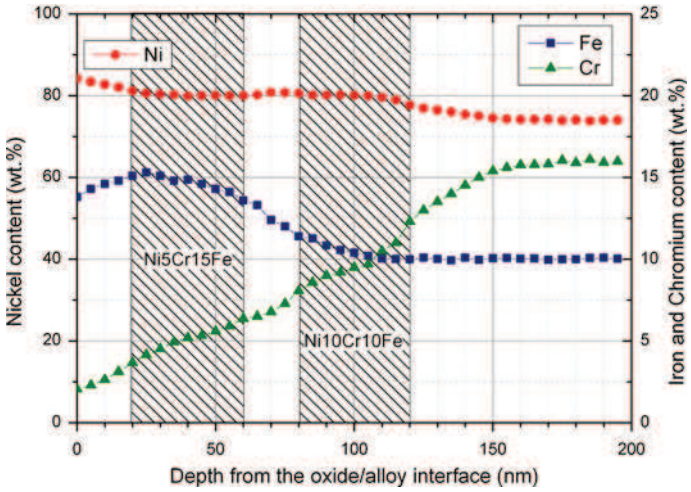

Fig. 1 EDX profiles performed on TEM cross-section of Alloy 600 after an exposure in primary water (360 °C) during 300 h (adapted from [9])

Table 1 Chemical composition of studied alloys (wt%)

	Ni	Cr	Fe	Al	Ti	Cu	C	Si	Mn
Alloy 600	Bal.	16.05	9.8	0.25	0.03	0.02	0.034	0.20	0.08
Ni10Cr10Fe	Bal.	10.02	10.55	0.12	<0.005	0.013	0.027	0.107	0.074
Ni5Cr15Fe	Bal.	4.98	15.38	0.14	<0.005	0.024	0.025	0.081	0.122

heterogeneous grain size (ASTM grain size numbers from 4 to 10). Only intergranular chromium carbides were observed.

The synthetic NiFeCr ternary alloys were prepared by the research centre of Imphy Alloys with a strictly controlled processing route. The cast ingots, obtained by vacuum induction melting, were hot rolled down to the thickness of 5–6 mm. The microstructure of the ternary alloys was characterized by equiaxed small grains (ASTM grain size number = 8–9) and very few carbides (mainly intergranular).

The Young modulus (E) of each alloy was determined at 25 and 400 °C by tensile tests (Table 2). The tensile test method was composed by three cycles of loading/unloading in the elastic domain. The mechanical response obtained, showed that the Young modulus was not significantly different between the alloys studied

Table 2 Elastic properties of studied alloys: Young modulus at different temperatures (GPa)

	Ambient temperature 25 °C	400 °C (air)
Alloy 600	203 ± 5	182 ± 5
Ni10Cr10Fe	199 ± 5	184 ± 5
Ni5Cr15Fe	197 ± 5	176 ± 5

(The differences is less than five percent). Therefore, only a temperature dependency of the Young modulus E was used in the numerical computations.

High temperature X-ray diffraction measurements were carried out with D8 Advance X-ray diffractometer (Bruker AXS) using Cu-Kα radiation and a Pt heater. The measurements were performed in the 300–723 K temperature range, and in primary vacuum ($Po_2 \leq 10^{-4}$ bar). For all tested temperature, the diffraction patterns were obtained, after temperature stabilization, between 30° and 120° with 2θ configuration and with an angular step width of 0.02°. The lattice parameters and the thermal expansion coefficients (CTE) for each material were calculated from the diffraction patterns by pattern decomposition procedure with the DIFFRACplus EVA software (background subtracting, $K\alpha_2$-lines stripping, indexation by cell refinement…).

Finite element computations have been carried out on a rectangular sample of Alloy 600 (thickness 1 mm, width 3 mm and length 20 mm). Finite element calculations were performed with Cast 3 m finite element code [http://www-cast3m.cea.fr], in order to determine the local stress and strain tensor fields. The simulation was carried out using plane strain hypothesis using a 2D mesh (8 node-quadratic elements). Only half of the thickness was meshed because of plane symmetry. The depleted zone, as experimentally observed (Fig. 1) is 0.016 mm thick. The boundary conditions are the following: symmetry plane at the bottom side and the left side, free edge for the side of the affected zone; the right side is constrained to remain perpendicular to the plane of symmetry. Material behaviour remains elastic. Poisson's ratio is 0.28. The variation of the Young modulus was assumed linear with the temperature (200 GPa at 20 °C and 180 GPa at 400 °C).

Because of their dependency with Cr content, the material thermal properties used for calculation was described by the experimental data, as detailed in the results section.

As the stress state at high temperature is unknown, the Cr-depleted alloy is assumed in a first approach to be initially at 360 °C in a stress free state and the stress state generated by a cooling down to room temperature is calculated.

Results

For all the temperature tested, the average values of the lattice parameters assessed by cell refinement on the different indexed hkl-planes and for at least two sets of experience on each alloy are reported on Fig. 2. For the tested temperature range, a significant difference of lattice parameter is observable between Alloy 600 and the ternary alloys, while, as expected according to their Fe and Cr contents [14], it is similar for both ternary alloys. For the three alloys, the evolution of the lattice parameters is linear with the temperature. The slope is more pronounced for Alloy 600 than for the two ternary alloys. The CTE of Alloy 600 is higher ($13.2 \times 10^{-6}\ K^{-1}$) than the one of the ternary alloys ($8.7 \times 10^{-6}\ K^{-1}$ and $8.5 \times 10^{-6}\ K^{-1}$, respectively for Ni10Cr10Fe and Ni5Cr15Fe).

As a consequence of these results, FE simulations were carried out using CTE depending only on the Cr content. The simulation was performed with two different

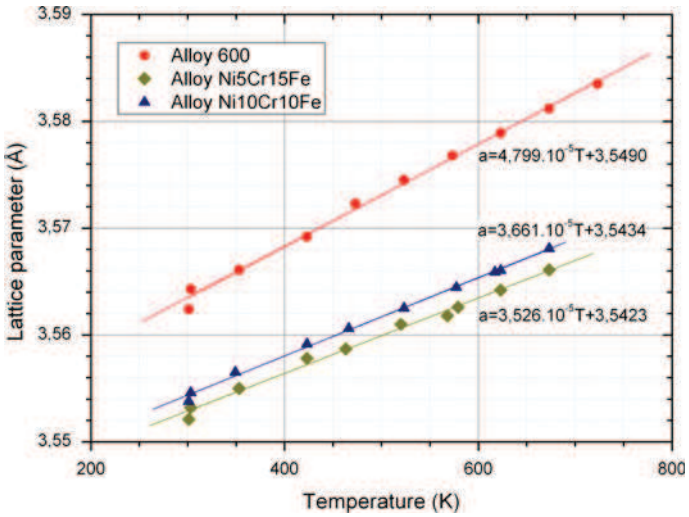

Fig. 2 Evolution of the lattice parameters with temperature for the alloys studied

CTE evolutions: a linear and another one fitted on an inverse cosines (Fig. 3). For both evolutions, a thermal strain gradient is observed when the sample is cooled down from 360 °C to ambient temperature. The thermal strain is larger at the Cr-depleted surface than in the bulk. Accordingly, a gradient of compressive stress parallel to the surface is observed in this Cr content transition zone. The extreme value, obtained at the Cr-depleted surface is −316 MPa with the linear dependence and −305 MPa with the inverse cosines one (Fig. 3). With our assumptions, the stress profile is directly linked to the CTE profile.

An simplified thermomechanical calculation, with the same volume proportion, was also done using Voigt two-element model: one element corresponding to Alloy 600 (CTE: 13.2 10–6 K^{-1}, E(T): 203–182) and the other to Cr-depleted zone (CTE: 8.6 10–6 K^{-1}, E(T): 200–180). However such simulation provides an overestimated stress state. Indeed, the extreme value of −405 MPa. Therefore, it is worth mentioning that to provide more relevant results, the contribution of the different Cr content layers properties to the whole structure mechanical loading need to be assumed.

Discussion

The local modification of the chemical composition in the underlying metal induces a noteworthy gradient of thermal properties, as well as mechanical properties. In the case of a Cr-depleted zone, the main influence is observed on CTE as the variation of the Young modulus with the chromium content is less than 5 %. The occurrence of such a CTE gradient may induce a significant stress level when the structure is submitted to temperature variation. In the present case, the stress state providing by

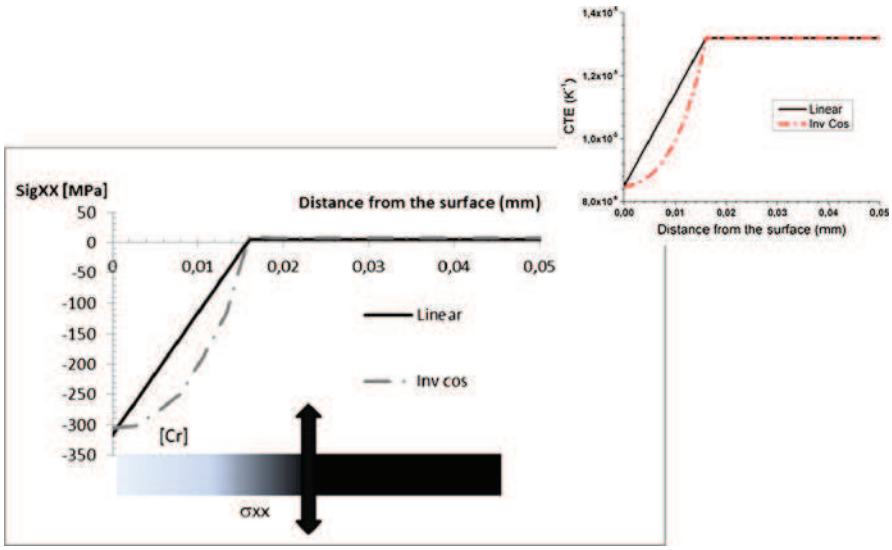

Fig. 3 Calculated distribution of the stress σxx (x is the direction parallel to the surface) after a cooling down from 360 °C to ambient temperature. The dependence of the CTE with the Cr content was taken into account

the Cr-depletion effect on a structure cooled down is shown to be a compressive stress gradient.

If the macroscopic scale is considered, this compressive stress gradient may be involved in the durability of the structure. Firstly, the most stressed part of the Cr-depleted zone is at the interface with the oxide layer. Moreover, at this interface, oxide growth also generates stresses. Therefore, taking into account all the previous features added with the oxide scale deformation with temperature, different situations seem possible. If the oxide scale remains in a tensile stress state larger than fracture strength, spallation or cracking of the oxide layer may occur. The occurrence of cracks into the oxide layer will involve, for further exposure (for example: cyclic test…) a localised corrosion phenomenon. Conversely, if the loading stress is lower than such a critical value, the oxide scale remains uncracked. Secondly, the compressive state of the surface of the metal after the cooling down may prevent the propagation of cracks providing from the Cr preferential oxidation. If some cracks had been generated during the high temperature exposure, their propagation will be slowed or even stopped by such compressive stress.

In this work, an unconstrained initial stress state in the Cr-depleted zone at 360 °C is assumed. However, the volume change induced by Cr-depletion at this temperature may lead also to a distribution of stresses in relation with the microstructural state [6]. At 360 °C, the recovery of such stress state is not evidenced. Zhou et al. [15], by computation with a continuum thermodynamic model implemented in FE, assessed to the stress state induced by Cr-depletion in a 16Cr-Fe alloys oxidized at 800 °C either in the oxide and the metal. They showed that the metal Cr-depleted sublayer is loaded by compressive and tensile stresses (up to 600 MPa). They supposed that the compressive

contribution is due to the oxide expansion at high temperature while tensile contribution is directly link to the Cr-depletion. These tensile stresses were assumed to assist or promote intergranular cracking at high temperature. Therefore, the level of tensile stresses generated during Cr-depletion must be assessed and compared to the stress state due to CTE mismatch.

To go further, a polycrystalline approach may be useful to describe the final stress state. Firstly, Zhou et al. [15] showed that at high temperature tensile stress was higher at grain boundaries than in the bulk. Secondly, regarding to the polycrystal scale, each grain of the exposed surface is affected by the Cr-depletion. As a consequence, stress state due to volume change needs to be taken into account for each grain. Stress accommodation between neighbouring grains is closely dependant of the grain size and of the local texture of the alloy, especially the relative orientations of neighbouring grains. A specific disorientation between two grains may generate locally a significant tensile stresses at the grain boundary. This phenomenon may be emphasized during thermal loading. Such stresses may then promote cracks initiation or propagation. Conversely, another distribution of disorientation angles may provide a compressive stress at the grain boundary and then prevents the intergranular cracking process. Therefore, it seems possible that the stress states due to volume change at 360 °C and to the difference of CTE may be locally cumulated or subtracted entailing preferential site to initiate IGSCC.

However, it is worth mentioning that some other features of the corrosion process may get involved into the local mechanical behavior at high temperature as well as during the cooling down. For example, intergranular oxide penetrations generate not only other stresses at grains boundaries but also other Cr-depletion phenomena at their vicinity [12, 13] which may also contribute to the stress state. Another contribution may be induced by the presence of hydrogen resulting from the corrosion process which may act on the cohesive stress at the vicinity of crack tip or intergranular penetration tip and more particularly during the cooling down when the hydrogen embrittlement becomes more detrimental. Therefore, to estimate the role of the Cr-depletion in IGSCC process, further studies taking into account the local coupling between the different stress contributions are required.

Finally, it is important to specify that for long term exposure, the Cr-depleted zone shrinks up to totally disappear [16]. Therefore, the stress state at the sublayer is time dependent: firstly during the formation of Cr-depleted zone and secondly during the long term dissolution of the matrix. This tendency indicates that the Cr-depletion contribution to IGSCC is relevant for the first stage of exposure. Therefore, to avoid the initiation of cracks, the control of the stress state generated by the volume change is a possible issue. Such control is possible if the Cr-depletion mechanism is managed in terms of Cr diffusion, Cr preferential oxidation kinetics and also other alloying elements behavior during this phenomenon.

Conclusions

The presented results confirm that the Cr-depletion occurring during the oxidation of Ni-base alloys in high temperature water generate volume change and thermal

properties variation. Such modifications provide a noticeable stress state during the exposure but also during temperature variation. It is assumed that those stresses are one of the driven forces for IGSCC mechanism. These first results encourage us to go further in this study by developing a polycrystalline approach of the Cr-depletion taking into account the different origin of stresses (mechanical, chemical, environmental…) from the substrate and from the oxide layer.

Acknowledgments The authors would like to acknowledge AREVA Group for the materials supply and its financial support.

References

1. M. T. Miglin and H. A. Domian, *Journal of Material Engineering* **9**, 1987 (113).
2. R. H. Jones and S. M. Bruemmer, in *Proceeding of the 1st International Conference on Environment-Induced Cracking of Metals*, Kholer, eds. R. P. Gangloff et al. (NACE), pp.287 (1988).
3. G. S. Was and D. J. Paraventi and J. L. Hertzberg, *Corrosion-Deformation Interactions CDI'96*, Nice, eds. T. Magnin and J.M. Gras (les editions de physique) pp.410 (1996).
4. P. M. Scott and M. Le Calvar, in *Proceeding of 6th International Symposium on Environmental Degradation of Materials in Nuclear Power System-Water Reactors* (TMS-ANS), pp.657 (1993).
5. P. M. Scott and M. Le Calvar, *Corrosion-Deformation Interactions CDI'96*, Nice, eds. T. Magnin et J. M. Gras (les editions de physique, 1996) pp.384.
6. P. Combrade and P.M. Scott and M. Foucault and E. Andrieu and P. Marcus, in *Proceeding of 12th International Symposium on Environmental Degradation of Materials in Nuclear Power System—Water Reactors*, Salt Lake City, eds T.R Allen et al. (TMS), pp.883 (2005).
7. B. Ter-Ovanessian and J. M. Cloué and J. Deleume and E. Andrieu, in *Proceeding of 14th International Symposium on Environmental Degradation of Materials in Nuclear Power System—Water Reactors*, Virginia Beach (ANS), pp.99 (2009).
8. C. Soustelle and M. Foucault and P. Combrade, and K. Wolski and T. Magnin, in *Proceeding of 9th International Symposium on Environmental Degradation of Materials in Nuclear Power Systems—Water Reactors,* Newport Beach, eds. S.M. Bruemmer et al. (TMS), pp.105 (1999).
9. J. Panter, "Etude de la corrosion sous contrainte des alliages 600 et 690 en milieu primaire de réacteur à eau sous pression (REP)—Influence des procédés de fabrication des tubes de générateurs de vapeur sur la phase d'amorçage" PhD Thesis, Institut National Polytechnique de Toulouse, 2002.
10. J. Panter, B. Viguier, J. M. Cloué, M. Foucault, P. Combrade and E. Andrieu, *Journal of Nuclear Materials* **348**, 2006 (213).
11. F. Carette, M. C. Lafont, G. Chatainier, L. Guinard and B. Pieraggi, *Surface Interface Analysis* **34**, 2002 (135).
12. P. Laghoutaris, "Corrosion sous contrainte de l'alliage 600 en milieu primaire des réacteurs à eau sous pression: apport à la comprehension des mécanismes", PhD Thesis, Ecole Nationale Supérieure des Mines de Paris, 2009.
13. L. E. Thomas and S.M. Bruemmer, *NACE Corrosion* **56** 6 (2000) paper#00060572.
14. G. P. Sabol and R. Stickler, *Physica Status Solidi* **39**, 1969 (11).
15. H. Zhou, J. Qu and M. Cherkaoui, *Computational Materials Science* **48**, 2010 (842).
16. P. Combrade, Communication, *Ecole thématique Corrosion et Protection des Matériaux à Haute Température, CorroHT'10*, Porquerolles (2010).